JGR Oceans

RESEARCH ARTICLE
10.1029/2020JC017063

Special Section:
Uncovering the hidden links between dynamics, chemical, biogeochemical and biological processes under the changing Arctic

Key Points:

- The trophic level of *Calanus hyperboreus* was correlated with the proportion of fatty acid marker of diatom between two contrasting areas
- The likely driver of this was variations in phytoplankton community related to stratification caused by sea ice meltwater inflow in summer
- *C. hyperboreus* could be an indicator organism to understand trophic dynamics in zooplankton food web in the Arctic Ocean

Supporting Information:

- Supporting Information S1

Correspondence to:
K.-H. Shin,
shinkh@hanyang.ac.kr

Citation:
Choi, H., Won, H., Kim, J.-H., Yang, E. J., Cho, K.-H., Lee, Y., et al. (2021). Trophic dynamics of *Calanus hyperboreus* in the Pacific Arctic Ocean. *Journal of Geophysical Research: Oceans*, *126*, e2020JC017063. https://doi.org/10.1029/2020JC017063

Received 12 DEC 2020
Accepted 26 FEB 2021

Trophic Dynamics of *Calanus hyperboreus* in the Pacific Arctic Ocean

Hyuntae Choi[1], Haemin Won[1], Jee-Hoon Kim[2], Eun Jin Yang[2], Kyoung-Ho Cho[2], Youngju Lee[2], Sung-Ho Kang[2], and Kyung-Hoon Shin[1]

[1]Department of Marine Sciences and Convergent Technology, Hanyang University, Ansan, South Korea, [2]Division of Ocean Sciences, Korea Polar Research Institute (KOPRI), Incheon, South Korea

Abstract The zooplankton community composition in the Pacific Arctic Ocean depends heavily on the sea ice and hydrodynamic conditions. The calanoid copepod *Calanus hyperboreus* is a dominant Arctic zooplankton, but its diet sources in the Pacific Arctic are unclear. *C. hyperboreus* individuals were collected in the northern Chukchi Sea (NCS) and the northern-East Siberian Sea (NESS), which display contrasting chlorophyll abundance and sea ice concentration in summer 2018. Nitrogen isotopes of individual amino acid and fatty acid compositions were measured to determine its trophic level (TL) and dominant diet. *C. hyperboreus* collected in the NCS had higher TL values (3.0 ± 0.2) and a relatively low proportion of C20:5(n-3). In the NESS, *C. hyperboreus* had lower TL values (2.7 ± 0.2) and a larger percentage of C20:5(n-3), suggesting a greater proportion of diatoms in its diet. Spatial TL variations of *C. hyperboreus* between the NCS and NESS may be caused by variations in phytoplankton composition (micro-phytoplankton vs. nano- and picophytoplankton) as a result of surface seawater stratification triggered by the inflow of sea ice meltwater as well as summer Bering Sea water through the Bering Strait. These results suggest that the filter-feeding copepod *C. hyperboreus* could be a useful indicator to understand trophic dynamics in zooplankton food web.

Plain Language Summary The Pacific region of the Arctic Ocean experiences different annual volumes of freshwater inflow, resulting in changes to its water-mass structure. In 2018, we harvested *Calanus hyperboreus*, a dominant Arctic zooplankton, from the northern Chukchi Sea (NCS) and northern-East Siberian Sea (NESS). Sea ice concentrations and phytoplankton abundance varied between the regions. We analyzed the fatty acid composition and amino acid nitrogen isotope ratios to determine its diet sources and trophic dynamics, respectively. We found that *C. hyperboreus* collected in the NCS occupied higher trophic levels and had a low proportion of diatom-marker fatty acids. In contrast, in the NESS, *C. hyperboreus* occupied lower trophic levels and had a larger percentage of diatom-marker fatty acids, suggesting diatom accounted for a large portion of its diet in the NESS compared with the NCS. Analysis of amino acid nitrogen isotope and fatty acid composition of *C. hyperboreus* revealed a shift in trophic levels and diets, respectively.

1. Introduction

The Pacific Arctic Ocean receives relatively warm and nutrient-rich Pacific summer water inflow via the Bering Strait and the Chukchi Sea. The East Siberian Sea, which is productive and shallow, is situated in the western part of the Pacific Arctic Ocean (Semiletov et al., 2005). In the eastern region, the northern Chukchi Sea, which is poor surface nutrient and have deep basin, is partially located at the surrounding area of the anticyclonic Beaufort Gyre (Coupel et al., 2015). The Pacific Arctic Ocean exhibits rapid responses to environmental change. Strong stratification is caused by incoming sea ice meltwater in summer (McLaughlin et al., 2011). The nutricline and surface chlorophyll maximum (SCM) depth can be deepened by stratification, decreasing primary productivity due to limited nutrient supplies (Coupel et al., 2015; Zhuang et al., 2018). The zooplankton community is tightly tied to the hydrodynamic condition and depends on the composition of their diets. In low-nutrient conditions and a stable water column, smaller phytoplankton such as pico- and nanoplankton are usually dominant (Coupel et al., 2012; He et al., 2012; Li et al., 2009). Whereas, diatom was dominant under high sea ice concentration in nutrient-rich and vertically mixed water column (Lee et al., 2019). The composition of primary producers, the cell sizes of which vary widely, influences the available diet for higher consumers, such as microzooplankton (Matsuno et al., 2014; Yang et al., 2015).

The relationship between Arctic phytoplankton and zooplankton has been reported using feeding experiments (Campbell et al., 2016, 2009), gut content analysis (Kruse et al., 2010), fatty acid composition (McMeans et al., 2012), and stable isotope analysis (Grigor et al., 2015; Søreide et al., 2008). Stable isotope and fatty acid analysis can provide helpful information on assimilated food sources over a period of two weeks (Graeve et al., 2005). Major algal diets of zooplankton are characterized by the typical fatty acids markers for diatoms (eicosapentaenoic acid [EPA; C20:5(n-3)]) and dinoflagellates (docosahexaenoic acid [DHA; C22:6(n-3)]), both of which are essential for growth and reproduction (Falk-Petersen et al., 2009). The nitrogen isotope ratio (δ^{15}N) can provide trophic information, which generally have elevation of 3‰–4‰ per trophic transfer (Minagawa & Wada, 1984; Søreide et al., 2006). More recently, compound-specific isotope analysis of amino acids (CSIA-AA) has been used to obtain detailed information in ecological and biogeochemical studies (Ohkouchi et al., 2017). Nitrogen isotopes of an individual amino acid ($\delta^{15}N_{AA}$) offer useful information on the trophic structure of the food web by estimating the trophic level (TL_{AA}) of consumers (McMahon & McCarthy, 2016). Trophic elevation can be characterized as trophic amino acids (AAs), which have large δ^{15}N enrichment (3‰–8‰), and the isotopic baseline in food webs can be explained by source AAs that show reduced δ^{15}N enrichment (0‰–1‰). The TL_{AA} of the organism can be calculated by the nitrogen isotope ratio of glutamic acid ($\delta^{15}N_{Glu}$) and phenylalanine ($\delta^{15}N_{Phe}$) as trophic and source AAs, respectively (Chikaraishi et al., 2009). The TL_{AA} value can be independent of the nitrogen isotope ratio at the δ^{15}N baseline regardless of basal food source sampling (Bowes & Thorp, 2015). The TL_{AA} value estimated by the CSIA-AA method can be accurate despite large variations in the δ^{15}N baseline in the food web (Hannides et al., 2009).

Calanus hyperboreus is a dominant calanoid copepod in the Arctic Ocean, and plays an important role in linking primary production to higher consumers (Conover, 1988). *C. hyperboreus* and other *Calanus* species filter-feed primarily on phytoplankton, sea ice algae, organic particles, and zooplankton larva (Cleary et al., 2017; Falk-Petersen et al., 2009; Frost, 1972). Some calanoid copepods can consume small phytoplankton (pico- or nanoplankton) (Boyd, 1976; Huntley & Tande, 1987) and protozooplankton (Cleary et al., 2017), exhibiting their available diet is coupled to the composition of organic particles in the water column. Several studies have focused on the seasonality of diet contents of calanoid copepods in the Arctic (McMeans et al., 2012; Søreide et al., 2008, 2010). However, in spite of the wide distribution of *C. hyperboreus* in the Arctic Ocean, little is known about their responses to variations in food sources among different water masses.

To evaluate the trophic dynamics of *C. hyperboreus* and its diet sources in different hydrographic conditions, we collected particulate organic matter (POM) and bulk tissue of *C. hyperboreus* individuals from the northern Chukchi Sea (NCS) and northern-East Siberian Sea (NESS), each of which had distinct physico-chemical conditions in 2018. The stable isotopes of the POM and bulk tissue of *C. hyperboreus* were analyzed, and amino acid nitrogen isotope values of *C. hyperboreus* were determined. Fatty acid compositions of *C. hyperboreus* were measured and compared between the NCS and NESS. We estimated TL_{AA} values of *C. hyperboreus* using isotopic differences between $\delta^{15}N_{Glu}$ and $\delta^{15}N_{Phe}$. TL_{AA} values of *C. hyperboreus* were compared between the NCS and NESS to determine the relationship between trophic dynamics and hydrography.

2. Materials and Methods

2.1. Sample Collection and Processing

Sampling was carried out during an August 2018 cruise of the Korean Icebreaker IBRV ARAON (ARA09B; August 4–August 26). Sampling stations and locations are displayed in Figure 1 and Table 1. The temperature, salinity, and density of seawater were measured with an SBE911plus conductivity-temperature-depth profiler with an SBE32 carousel water sampler. The accuracies for the T and C sensors are ±0.001°C and ±0.0003 S/m, respectively. Salinity data were corrected with bottle-sampled water using a Guildline 8400B autosalinometer. The stratification index was estimated as the density difference between the surface and a depth of 100 m (Coupel et al., 2012). The mixed layer depth was determined at the depth which showing over 0.05 kg/m^3 of density difference from 5 m depth (Lee et al., 2019). The monthly mean (August 2018) of

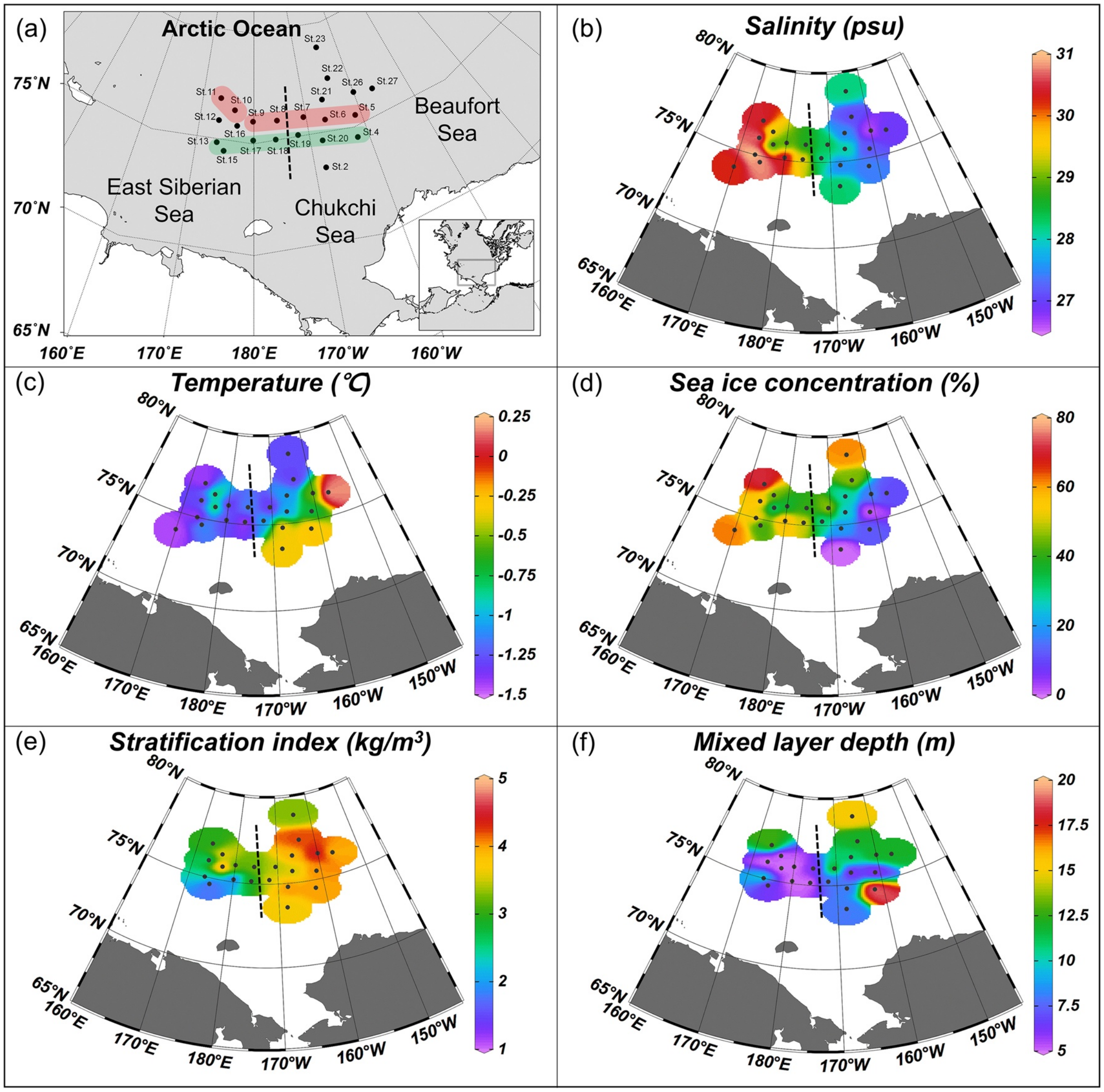

Figure 1. Study sites of this study (a) and their surface salinity (b), surface temperature (c), sea ice concentration (d), stratification index (e), and mixed layer depth (f). Red and green shaded area on (a) are transects described in Figure 3. Black dashed lines in each subfigure are for separating NESS and NCS. NCS, northern Chukchi Sea; NESS, northern-East Siberian Sea.

sea ice concentration, with a 3.125 km resolution, was obtained from a sea ice data archive (https://seaice.uni-bremen.de/data/amsr2) provided by the University of Bremen (Spreen et al., 2008). Total and micro (>20 μm) chlorophyll *a* were sampled and measured by protocols described previously (Lee et al., 2019). We used both surface (1–2 m) and euphotic layer depth-integrated chl *a* concentration (depth of each station is described in Table 1). Heterotrophic dinoflagellate (HDF) and ciliate abundance were determined following a previously described protocol (Jiang et al., 2013; Yang et al., 2015).

For POM collections, 4 L of surface water was filtered through a Whatman GF/F glass-fiber filter pre-combusted at 450°C for 4 h. Zooplankton samples were collected at each station with a bongo net (500 μm mesh size, 60 cm diameter) at a vertical velocity of 60 m/min from the surface to a depth of 200 m. Female *C. hyperboreus* adults were separated from the zooplankton assemblage. All POM and *C. hyperboreus* samples were stored at −80°C in a deep freezer. All samples were freeze-dried for 24 h. The prosome length and dry mass of *C. hyperboreus* individuals were carefully measured (Table S1), and all samples were stored at −20°C in a freezer before further preparation.

Table 1
Detailed Information of Sampling Stations

Location	Station	Latitude (°N)	Longitude (°W)	Water depth (m)	Euphotic layer depth (m)
NESS	8	76.00	−175.50	2018	100
	9	76.00	−180.00	1127	100
	10	76.50	176.50	991	100
	11	77.00	173.60	759	100
	12	75.00	173.60	268	100
	13	74.64	174.92	106	100
	15	75.80	177.06	69	60
	16	75.15	−180.00	558	100
	17	75.15	−176.00	593	100
	18	75.24	−171.97	372	100
NCS	2	73.58	−168.28	126	100
(melted)	4	74.52	−161.93	1709	100
	5	75.50	−161.13	2093	100
	20	74.80	−167.90	229	100
	26	76.50	−160.00	1970	100
	27	76.33	−156.38	705	100
NCS	6	75.69	−166.64	331	100
(frozen)	7	76.00	−170.50	1325	100
	19	75.24	−171.97	540	100
	21	76.60	−166.30	694	100
	22	77.47	−164.12	301	100
	23	78.95	−164.63	1789	100

NCS, northern Chukchi Sea; NESS, northern-East Siberian Sea.

2.2. Fatty Acid Analysis

The fatty acid composition of *C. hyperboreus* was measured following a protocol described by (Folch et al., 1957) with minor modifications (Lee et al., 2020). Total lipids were extracted from *C. hyperboreus* individuals ($n = 1$ for each station) with dichloromethane/methanol 2:1 (v/v). Nonadecanoic acid (C19:0) was added as a surrogate. Samples were sonicated, and organic phases were separated in triplicate. The lipid fraction was extracted from the water-methanol phase. Samples were saponified using KOH (0.5 M in methanol) for 1 h at 60°C and methylated using BF-3 methanol for 10 min at 60°C for derivatization to fatty acid methyl esters (FAMEs). Concentrations of FAMEs were measured by gas chromatography (HP 7890A, Agilent Technologies, US) with a flame ionization detector using a DB-5MS column (60 m in length, with an inner diameter of 0.25 mm and film thickness of 0.25 μm). The initial oven temperature was 60°C, which was increased at a rate of 5°C/min to 320°C, at which it was maintained for 10 min. FAs were identified from the retention times of FAME standards (Supelco, US) and mass spectra from a gas chromatography equipped with mass spectrometer (HP-7820A, Agilent Technologies, US) in the analytical conditions described above. Methyl heneicosanoic acid (C21:0) was used as an internal standard. More detailed positions and numbers of double bonds within unsaturated FAs were checked by 4,4-dimethyloxazoline (DMOX) derivatization with 2-amino-2-methylpropanol at 180°C for 24 h (Garrido & Medina, 1994; Spitzer, 1996). DMOX derivatives were analyzed and identified using mass spectra from GC/MS analysis.

2.3. Stable Isotope Analysis of Bulk Tissue

Stable isotope analysis was carried out using an elemental analyzer (Vario Select, Elementar, Germany) equipped with an isotope ratio mass spectrometer (Vision, Elementar, Germany). The whole bodies of single copepod individuals ($n = 1$ for each station) were homogenized. Approximate weights (0.6–1.0 mg) in samples were used for nitrogen isotope (δ^{15}N) analysis. Prior to carbon isotope (δ^{13}C) analysis, POM samples were exposed to 12 N HCl fumes for 20 h to remove inorganic carbon. For carbon isotope (δ^{13}C) analysis of *C. hyperboreus*, inorganic carbon was removed by 1 M HCl, and lipid contents were removed using 2:1 chloroform/methanol (v/v), with 0.2–0.7 mg samples subjected to δ^{13}C analysis. Due to the limited amounts of samples, all samples were analyzed without replication. Stable isotope ratios were displayed in conventional δ notation:

$$\delta X = \left[\left(\frac{R_{\text{Sample}}}{R_{\text{Standard}}}\right) - 1\right] \times 1000,$$

where X indicates δ^{13}C or δ^{15}N and R is the corresponding ratio of ^{13}C/^{12}C or ^{15}N/^{14}N. To determine the precision of isotope analysis, international standards (IAEA CH-3 and N-1) were used for δ^{13}C and δ^{15}N analysis, respectively. Stable isotope ratios of standards were measured every 10 samples. At whole analysis sets, their standard deviations were less than ±0.1‰ and ±0.2‰ for δ^{13}C and δ^{15}N, respectively.

2.4. Amino Acid Nitrogen Isotope Analysis

For analysis of amino acid nitrogen isotopes, a *C. hyperboreus* individual from each station ($n = 1$) was hydrolyzed for 20 h with 6 M HCl at 110°C. Hydrophobic contents were removed by 3:2 n-hexane/dichloromethane (v/v), and residual HCl was dried with N_2 gas at 70°C. After derivatization into N-pivaloyl-AA-isopropyl ester with 1:4 thionyl chloride/2-propanol (v/v) and 1:4 pivaloyl chloride/dichloromethane (v/v) in sequence, AA derivatives were extracted with 3:2 n-hexane/dichloromethane (v/v). All AA derivatives were stored in dichloromethane at −20°C before analysis. Amino acid nitrogen isotopes were analyzed with a gas chromatograph (HP 6890N, Agilent Technologies, US) connected to a combustor (GC5 Interface, Elementar, Germany) and an isotope ratio mass spectrometer (Isoprime, Elementar, Germany). The δ^{15}N-certified amino acid standards were purchased from SHOKO-Science and Indiana University. We used a derivative of a standard mixture of 9 amino acids (alanine, glycine, valine, leucine, norleucine, aspartic acid, methionine, glutamic acid, and phenylalanine). In the calibration procedure, δ^{15}N values of all amino acid standards exhibited a standard deviation of less than ±1‰.

All TL_{AAs} were estimated using the following equation (Chikaraishi et al., 2009):

$$TL_{AAs} = \left[\left(\delta^{15}N_{Glu} - \delta^{15}N_{Phe} - 3.4\right) / 7.6\right] + 1$$

where $\delta^{15}N_{Glu}$ and $\delta^{15}N_{Phe}$ are the nitrogen isotope ratios of glutamic acid (Glu) and phenylalanine (Phe), respectively. The 3.4 (β value) is an empirical value of the isotopic difference between Glu and Phe in primary producers. A 7.6‰ trophic enrichment factor is applied to the δ^{15}N enrichment of Glu relative to phenylalanine with each trophic transfer.

2.5. Statistical Analysis

Independent t-tests were conducted to determine differences in the analytical data of *C. hyperboreus* collected from the NCS and NESS in a 95% confidence interval. The spatial difference of prosome length, body weight, FA composition, bulk carbon, bulk nitrogen, and amino acid nitrogen isotopes of *C. hyperboreus* in the NCS and NESS were compared using t-tests. Additionally, hydrographic parameters (temperature, salinity, density, mixed layer depth, stratification index, and sea ice concentration) between two regions were compared by *t*-tests. All statistical analysis was conducted by IBM SPSS software v23.0.

3. Results

3.1. Hydrography and Biology in Study Sites

The NCS and NESS group were divided by east-west salinity difference of surface water along longitude, with relatively lower salinity in NCS (<28.5 psu) surface water compared with the NESS (Figures 2a and 2b). Relatively lower salinity and sea ice concentrations were detected in the eastern part of the NCS, indicating more sea ice had melted. We then separated relatively ice-melted (<20% of sea ice concentration) and frozen areas (>20% of sea ice concentration) within NCS stations based on sea ice concentration. Between the NESS and NCS, there were significant differences in temperature, salinity, density, and sea ice concentration (Table S1). The NCS showed relatively warmer surface water temperature (−0.755 ± 0.492°C) compared to those (−1.207 ± 0.239°C) in the NESS (Figures 3a and 3b). A strong halocline was discovered with low salinity (<28.5 psu) in the NCS (Figures 3c and 3d). The stratification index and mixed layer depth was slightly lower and deeper in the NESS compared to the NCS (Figures 1e and 1f). Additionally, chlorophyll *a* concentration was associated with a different spatial variation. In the northern transect, strong sub-SCM layers were observed at depths of 15–40 m in the NESS (Figure 3e). In the southern transect, a high concentration of chl *a* was found at depths of 0–20 m in the NESS (Figure 3f), while weak SCM layers appeared at depths of 30–50 m in the NCS. The NESS stations showed high sea ice concentration ranging from 32% to 71%, while the NCS stations reported mostly sea ice concentration below 50%. Sea ice concentration were not clearly separated from NCS and NESS. Rather, sea ice concentration was positively correlated with latitude (Figure 2c).

Average concentrations of total and micro-chl *a* were higher in the NESS than in the NCS (Table 2). Such a difference in biomass between two areas could be also observed in a protozooplankton group, with a greater number of individuals of heterotrophic dinoflagellates and ciliates in the NESS than in the NCS (Table 2). Between ice-melted and frozen areas within the NCS, there were no significant differences in heterotrophic dinoflagellates, ciliate abundances, and surface chl *a* concentrations. However, depth-integrated chl *a* concentrations differed significantly between the two areas within the NCS. The melted area in the NCS had higher depth-integrated chl *a* concentrations compared with the frozen area of the NCS.

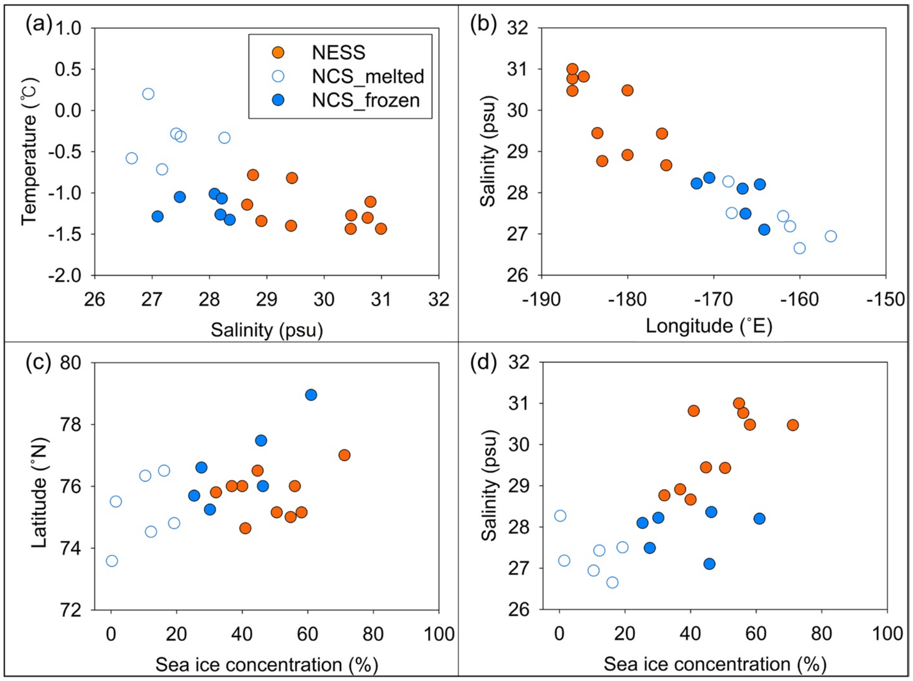

Figure 2. Distribution of surface temperature, surface salinity, and sea ice concentration at sampling stations.

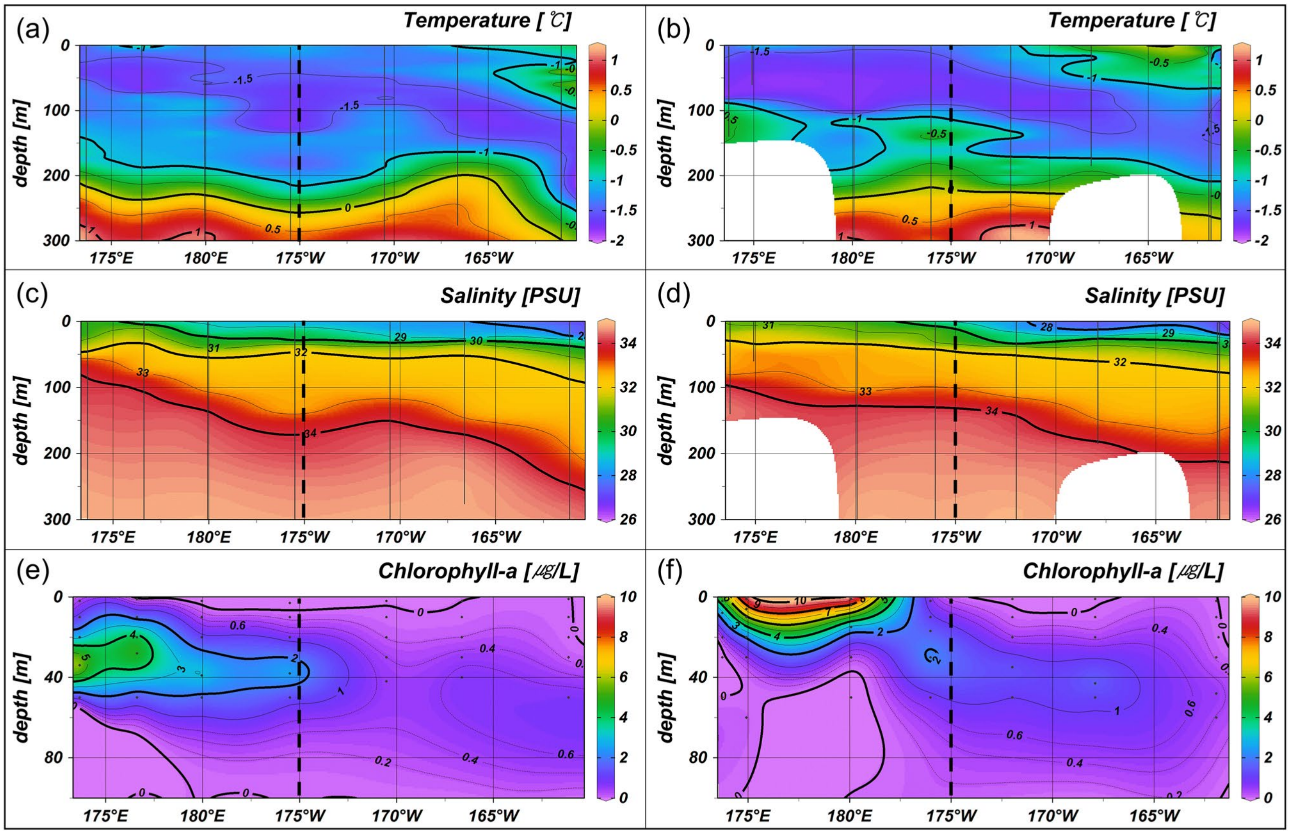

Figure 3. Vertical profile of temperature (a), (b), salinity (c), (d), and total chlorophyll *a* (e), (f) in two different transects (a, c, and e for red-shaded area and b, d, and f for green-shaded area in Figure 1a, respectively). Black dashed lines in the middle of each subfigure are for separating NESS and NCS. NCS, northern Chukchi Sea; NESS, northern-East Siberian Sea.

Table 2
Averaged Abundance of Total chl a (Surface), Micro-chl a, Heterotrophic Dinoflagellates, and Ciliates in the NCS and NESS in August 2018

		NESS	NCS (melted)	NCS (frozen)
Total chl *a*	Surface (μg/L)	3.17 ± 3.90	0.03 ± 0.01	0.04 ± 0.01
	Depth-integrated (mg/m^2)	93.52 ± 26.52	44.75 ± 58.14	22.17 ± 7.93
Micro-chl *a*	Surface (μg/L)	2.88 ± 3.62	0.01 ± 0.01	0.02 ± 0.02
	Depth-integrated (mg/m^2)	82.76 ± 27.14	26.78 ± 61.80	9.93 ± 9.44
Heterotrophic dinoflagellates (cells/L)		1741.55 ± 1160.01	327.00 ± 345.59	265.33 ± 170.46
Ciliate (cells/L)		476.64 ± 447.48	64.00 ± 71.59	54.83 ± 38.26

Note. Data was provided by Korea Arctic Ocean data-system (KAOS, https://kaos.kopri.re.kr).
NCS, northern Chukchi Sea; NESS, northern-East Siberian Sea.

3.2. Fatty Acid Profiles of *C. hyperboreus*

Fatty acid concentrations and their relative proportions are displayed in Table S3 and S4, respectively. The mean total fatty acid (TFA) concentration of *C. hyperboreus* was significantly different, displaying 434.5 ± 71.1 mg/g and 240.6 ± 187.9 mg/g in the NESS and NCS, respectively (independent *t*-test performed at 95% confidence intervals, $p = 0.009$). The FA concentrations in the NCS stations ranged more widely than in the NESS stations (Figure 4). Monounsaturated fatty acid (MUFA) was the most abundant, accounting for more than 50% of the TFA in both the NESS and NCS (Table S4). Mean abundances of polyunsaturated fatty acid (PUFA) contents were higher in the NESS than in the NCS. In entire FAs, C16:1(n-9) was the most abundant compound in both the NESS and NCS, with an average proportion of 35.0 ± 5.3% and 33.3 ± 9.1%, respectively (Figure 4). C20:5(n-3) was the next most abundant, with a proportion of 17.6 ± 2.6% in the NESS. C20:1(n-9) was the second most abundant FA, with a percentage of 10.8 ± 3.5%, in the NCS. These two FAs exhibited a significant difference in relative proportions between the NESS and NCS. In contrast, the C22:6(n-3) proportion showed an unclear statistical difference between both areas. Among specific FAs markers between the NESS and NCS, C15:0, C18:1(n-9), and C20:5(n-3) displayed significant spatial variation (Figure 5). Within the NCS stations, stations 06, 07, and 19 had the highest FAs concentrations. But in both concentration and relative proportion, most differences between melted and frozen NCS areas were insignificant.

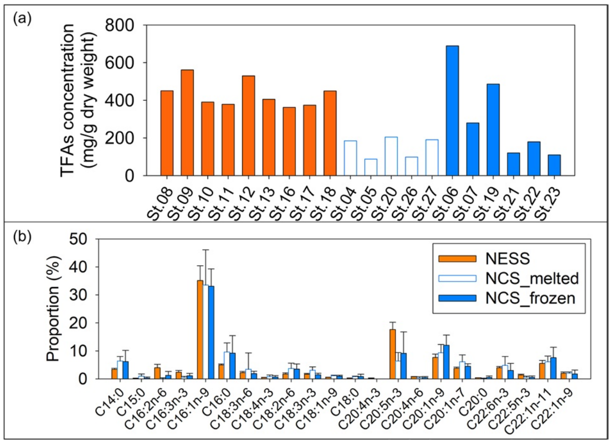

Figure 4. Total fatty acid concentration of *C. hyperboreus* at each sampling station (a) and relative abundances of fatty acids (b).

3.3. Bulk Carbon and Nitrogen Isotope Ratios

The δ^{13}C and δ^{15}N values for POM and *C. hyperboreus* were largely different between the NESS and NCS (Tables 3 and 4, Figures 6a and 6b). Average δ^{13}C and δ^{15}N values of POM were substantially lower in the NCS than in the NESS ($p = 0.000$ for both δ^{13}C and δ^{15}N). Average δ^{13}C values of *C. hyperboreus* were significantly higher in the NESS than in the NCS ($p = 0.001$, Figure 6). In contrast, lower δ^{15}N values for *C. hyperboreus* were evident in the NESS compared with the NCS ($p = 0.000$). In addition, no significant differences in δ^{13}C and δ^{15}N values were seen in either POM and *C. hyperboreus* between melted and frozen areas in NCS stations ($p > 0.05$).

3.4. Amino Acid Nitrogen Isotopes of *C. hyperboreus*

The $\delta^{15}N_{Glu}$ values of *C. hyperboreus* in NESS and NCS differed significantly, at 20.7 ± 1.4‰ and 22.5 ± 1.0‰, respectively ($p = 0.002$, Figure 6c). In contrast, the $\delta^{15}N_{Phe}$ values of *C. hyperboreus* varied within a similar range between the NESS (2.0–6.0‰) and the NCS (1.9–5.7‰) with insignificant variation ($p = 0.776$, Figure 6d). The estimated trophic level of *C. hyperboreus* was higher in the NCS (3.0 ± 0.2) than in the

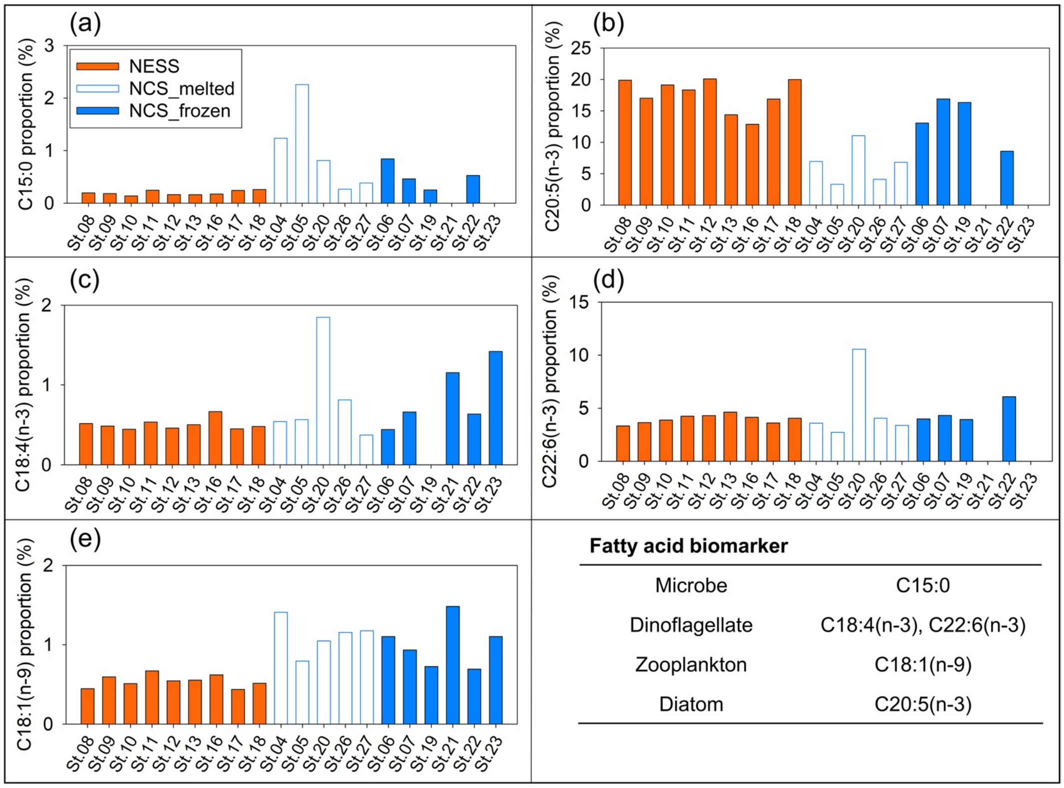

Fatty acid biomarker

Microbe	C15:0
Dinoflagellate	C18:4(n-3), C22:6(n-3)
Zooplankton	C18:1(n-9)
Diatom	C20:5(n-3)

Figure 5. Relative abundances of specific FAs markers of *C. hyperboreus* at each sampling station. Each compound is a common biomarker for specific organisms (Kelly & Scheibling, 2012).

NESS (2.7 ± 0.2) ($p = 0.007$, Figure 6e). In addition, a correlation was found between TL_{AA} values and body weights (Figure 7c). Neither latitude nor longitude had a clear correlation with TL_{AA} values ($R^2 = 0.066$ and $R^2 = 0.290$ for latitude and longitude, respectively). Between melted and frozen areas in the NCS stations, there were no significant difference in $\delta^{15}N_{Glu}$, $\delta^{15}N_{Phe}$, and TL_{AA} values.

4. Discussion and Summary

4.1. Hydrography in Study Area

Phytoplankton production in the Pacific Arctic Ocean usually depends on the water mass composition or sea ice concentration (Arrigo & van Dijken, 2015; Coupel et al., 2015). There are distinctly segregated water masses between NCS and NESS in this study. The warmer surface temperature can be attributed to the Pacific summer water inflow or solar irradiation (Figures 3c and 3d). Low salinity (<28.5 psu) in surface water in the NCS stations was observed, while the NESS stations showed relatively higher salinity. Lower salinity in NCS surface waters indicated relatively more input from riverine water and sea ice meltwater. Such differences of temperature and salinity result distinct spatial distribution of stratification index and mixed layer depth (Figures 1e and 1f). The stratification index larger than 3.0 kg/m^3 has been observed in the Pacific Arctic, which sea ice has been mostly melted (Coupel et al., 2015; Tremblay et al., 2009). Chl *a* concentrations and protozooplankton (heterotrophic dinoflagellate and ciliate) biomass were higher in the NESS than in the NCS (Table 2). The spatial variations between the two areas, which are described in previous studies (Jiang et al., 2013; Lee et al., 2019; Yang et al., 2015), may be caused by differences in the depth of the halocline layer. Surface water in the NCS is stratified in summer by large volumes of sea ice meltwater triggered by the Beaufort Gyre, with a deepening nutricline and an inhibited vertical nutrient supply (McLaughlin & Carmack, 2010). The surface mixing layer of the NCS is usually nutrient-poor, resulting in small contributions of larger-sized phytoplankton, such as diatoms (Coupel et al., 2012; Joo et al., 2012). In contrast, picoplankton and small flagellates are dominant in the NCS (Yang et al., 2015).

Table 3
Bulk $\delta^{13}C$ and $\delta^{15}N$ (‰) Values of POM and C. hyperboreus in August 2018

			POM			*C. hyperboreus*	
Location	Station	*N*	$\delta^{13}C$	$\delta^{15}N$	*N*	$\delta^{13}C$	$\delta^{15}N$
NESS	8	1	−26.3	2.6	1	−23.2	7.1
	9	1	−25.5	3.5	1	−22.5	10.0
	10	1	−23.8	4.7	1	−21.8	7.5
	11	1	−25.0	4.9	1	−22.0	7.7
	12	1	−24.2	6.6	1	−20.4	7.4
	13	1	−25.1	4.7	1	−20.4	8.3
	14	1	−25.0	8.0			
	15	1	−21.3	8.1	1	−19.9	9.1
	16	1	−23.7	4.2			
	17	1	−22.9	7.5	1	−23.6	8.2
	18	1	−23.6	10.2	1	−22.5	7.7
Mean			−24.2	5.9		−21.8	8.1
SD			1.4	2.3		1.3	0.9
NCS	2	1	−26.1	4.8			
(melted)	4	1	−28.2	3.2	1	−24.1	12.0
	5	1	−28.9	1.8	1	−25.8	11.2
	20	1	−29.1	0.6	1	−23.1	12.0
	26	1	−29.4	1.0	1	−25.6	10.6
	27	1	−30.0	−0.1	1	−24.0	10.5
NCS	6	1	−27.8	2.1	1	−25.1	10.6
(frozen)	7	1	−27.4	2.7	1	−24.1	11.6
	19	1	−26.4	1.3	1	−22.1	8.4
	21	1	−28.5	1.2	1	−26.0	11.4
	22	1			1	−22.2	12.5
	23	1	−27.2	2.0	1	−24.4	14.2
Mean			−28.1	1.9		−24.2	11.4
SD			1.2	1.3		1.4	1.4
df			20	20		18	18
$t_{0.05}$			6.878	4.961		4.030	−5.828
p value			0.000*	0.000*		0.001*	0.000*

Note. Independent *t*-test results of each parameter between NCS and NESS are displayed on the bottom.

NCS, northern Chukchi Sea; NESS, northern-East Siberian Sea; POM, particulate organic matter.

Asterisk (*) indicates statistical significance between two locations ($p < 0.05$*).

The NESS is influenced by saline (<33 psu) and nutrient-rich water mass from East Siberian shelf (Anderson et al., 2017). Although the influence of such water mass to the NESS is varied yearly (Kim et al., 2021; Nishino et al., 2013), the diatom showed dominant contribution to the phytoplankton community in summer (Lalande et al., 2019; Lee et al., 2019). Such different hydrodynamic conditions could affect the composition of available diet sources for zooplankton in the NCS and NESS.

4.2. Fatty Acid Composition of *C. hyperboreus* and Its Potential Diets in the NESS and NCS

Zooplankton have evolved a species-specific ecological strategy to survive when available algal diets are depleted. Filter-feeding copepods can utilize a wide range of available dietary options. Cleary et al. (2017) reported *Calanus* can consume not only an algal diet but also protozooplankton and eggs of their predators. In the present study, *C. hyperboreus* showed a spatial difference in body weight between the NESS and NCS, even though their prosome lengths and stage development were similar (Table S1). Such differences in body weight between the NESS and NCS may be a product of the substantial differences in TFA concentrations (Figure 4). Our results showed TFA concentrations were closely correlated with body weight in *C. hyperboreus* (Figure 7a). In this study area, high chlorophyll *a* concentration and large phytoplankton (diatom) dominance was occurred in the NESS. But relatively low chlorophyll *a* concentration and small phytoplankton was abundant in the NCS. Larger copepods can have a chance to directly feed on the large phytoplankton in the NESS. Smaller copepods in the NCS may feed on not only small phytoplankton but also more protozooplankton which have ecologically higher trophic level. TFA concentrations in *C. hyperboreus* were higher in all NESS stations but not in NCS stations. Some of the frozen NCS stations (St. 06, St. 07, and St. 19) reported high TFAs concentrations in *C. hyperboreus*. But these stations in the NCS were adjacent to the NESS, and so the TFA concentrations in *C. hyperboreus* would be comparatively closer to the stations in the NESS compared with those in melted areas in the NCS.

In the FA pool, some FAs can be used as indicators for specific algal diet sources (i.e., C20:5(n-3) for diatoms). Even among the same species, the FA composition can differ according to the type of assimilated diet source. For example, *C. hyperboreus* collected in Cumberland Sound have dominant C16:1(n-7) and C20:5(n-3) (McMeans et al., 2012). On the other hand, C22:6(n-3) was the most abundant FA for *C. hyperboreus* and other *Calanus* species in Kongsfjorden (Scott et al., 2002). Dahl et al. (2000) reported that C20:5(n-3) and C22:6(n-3) in *C. hyperboreus* from Mijenfjorden have few (both less than 5%) TFAs. These differences were closely related to diet composition in the habitat environments because specific marker FA abundances provide the assimilated diet information. In particular, C15:0, which indicates microbial markers, and C18:1(n-9), which indicates a zooplankton diet, appeared at slightly higher proportions in some *C. hyperboreus* individuals from NCS stations (Figures 5a and 5e). In contrast, C20:5(n-3) concentrations were higher in *C. hyperboreus* from the NESS, suggesting more diet assimilation of diatom. A significant correlation between micro-chl *a* concentrations and the C20:5(n-3) contents of *C. hyperboreus* suggest that the micro-chl *a* pool should be dominated by diatoms with high C20:5(n-3) contents in *C. hyperboreus* (Figure 7b). However, small proportions of C22:6(n-3) and C18:4(n-3), which are dinoflagellate markers (Sargent et al., 1995), were found in both the NESS and NCS,

Table 4
$\delta^{15}N_{AAs}$ (‰) and TL_{AAs} Values of C. hyperboreus in August 2018

Location	Station	*N*	$\delta^{15}N_{Glu}$	$\delta^{15}N_{Phe}$	TL_{AAs}
NESS	8	1	20.1	5.5	2.5
	9	1	18.6	2.0	2.7
	10	1	19.3	2.4	2.6
	11	1	22.2	4.0	2.9
	12	1	20.2	3.6	2.7
	13	1	19.1	3.9	2.6
	15	1	22.8	3.3	3.0
	16	1	21.4	5.9	2.6
	17	1	22.1	6.0	2.7
	18	1	21.4	5.1	2.7
Mean			20.7	4.2	2.7
SD			1.4	1.4	0.2
NCS	2	1	20.1	2.8	2.8
(melted)	4	1	22.9	3.8	3.1
	5	1	23.4	4.0	3.1
	20	1	21.8	5.6	2.7
	26	1	22.6	1.9	3.3
	27	1	22.0	5.4	2.7
NCS	6	1	23.1	3.9	3.1
(frozen)	7	1	22.7	5.7	2.8
	19	1	21.7	5.5	2.7
	21	1	23.0	3.9	3.1
	22	1	22.9	4.8	2.9
	23	1	23.9	4.5	3.1
Mean			22.5	4.3	3.0
SD			1.0	1.2	0.2
df			20	20	20
$t_{0.05}$			−3.459	−0.289	−3.014
p value			0.002*	0.776	0.007*

Note. Independent *t*-test results of each parameter between NCS and NESS are displayed on the bottom.

NCS, northern Chukchi Sea; NESS, northern-East Siberian Sea.

Asterisk (*) indicates statistical significance between two locations ($p < 0.05$*).

demonstrating that dinoflagellate-derived diets can make small contributions to *C. hyperboreus* diets in both the NESS and the NCS. Therefore, *C. hyperboreus* in the NESS would feed on more algae compared with those in NCS.

4.3. Trophic Level of *C. hyperboreus* as the Filter Feeder

We found a longitudinal gradient of bulk $\delta^{13}C$ values for both POM and *C. hyperboreus*. Carbon stable isotopic ($\delta^{13}C$) differences between POM and *C. hyperboreus* at each station averaged 3.8 ± 1.3‰ and 2.4 ± 1.6‰ in the NCS and NESS, respectively, showing a range similar to those in previous reports (Søreide et al., 2008, 2006). In contrast, $\delta^{15}N$ values between POM and *C. hyperboreus* in the NCS showed a substantially large difference (9.7 ± 1.5‰) compared with the NESS (2.3 ± 2.6‰). This suggests that *C. hyperboreus* in the NCS involve higher steps of trophic transfers in the food web. In our data set, bulk $\delta^{15}N$ values in POM samples showed large spatial variations, ranging from 0‰ to 10‰. Such $\delta^{15}N$ baseline variation is a product of the magnitude of assimilation of various nitrogen sources (i.e., N_2, NO_3^-, and NH_4^+) during primary production (Chikaraishi et al., 2009). The trophic level estimated by $\delta^{15}N_{Glu}$ and $\delta^{15}N_{Phe}$ offer the advantage that such spatial variation of $\delta^{15}N$ baseline is normalized. Previous studies have elucidated trophic levels of single species of zooplankton using compound-specific $\delta^{15}N$ analysis of AAs. Hannides et al. (2009) suggested that the trophic level of a copepod depends on its body size and feeding behavior. The cyclopoid copepod, *Oithona* spp., positioned around a TL_{AA} of 2.0, likely consumes small and sinking particles and flagellates. However, the calanoid copepod *Euchaeta rimana*, which typically hunts larger and more mobile prey, displayed a TL_{AA} of close to 3.0. Our data set showed a wider range of TL_{AA} values of *C. hyperboreus,* from 2.5 to 3.3. A wide TL_{AA} range for *Calanus* was previously reported in Kongsfjorden, Svalbard (2.5–3.0 of $TL_{AA,}$ Choi et al. (2020)). High clearance on a wide range of diet size (20–200 µm) in cultivation experiments (Huntley & Tande, 1987; Levinsen et al., 2000) may contribute to varying TL_{AA} values for *C. hyperboreus*. The averaged TL_{AA} for *C. hyperboreus* in the NCS was higher than (0.3 units) that in the NESS. Body sizes and growth stages of *C. hyperboreus* were nearly identical between the NESS and NCS, but the body weight and TL_{AA} of *C. hyperboreus* displayed negative correlations between the NESS and NCS (Figure 7c). The TL_{AA} difference may be derived from the spatial variability of diet composition.

4.4. Trophic Dynamics of *C. hyperboreus* in the NESS and NCS

The TL_{AA} values of *C. hyperboreus* and its possible diets are provided in Figure 8. *C. hyperboreus* with a higher TL_{AA} showed small C20:5(n-3) contents, while *C. hyperboreus* with a lower TL_{AA} showed large C20:5(n-3) contents, with a significant correlation evident between specific FA contents and TL_{AA} values (Figure 7d). Our study showed small C20:5(n-3) contents for *C. hyperboreus* in the NCS, with lower total chl *a* concentrations, and lower concentrations of micro-chl *a* in particular. The main primary producers in the NCS would be smaller (nano or pico-sized) phytoplankton, accounting for 62.9% of the total chl *a* concentration. *C. hyperboreus* cannot feed directly on these smaller phytoplankton because even copepodites of *C. hyperboreus* showed poor clearance on a diet of algae smaller than 25 µm in diameter (Huntley & Tande, 1987). However, some protozooplankton that likely feed on small cells of primary producers were abundant in the NCS (Matsuno et al., 2014).

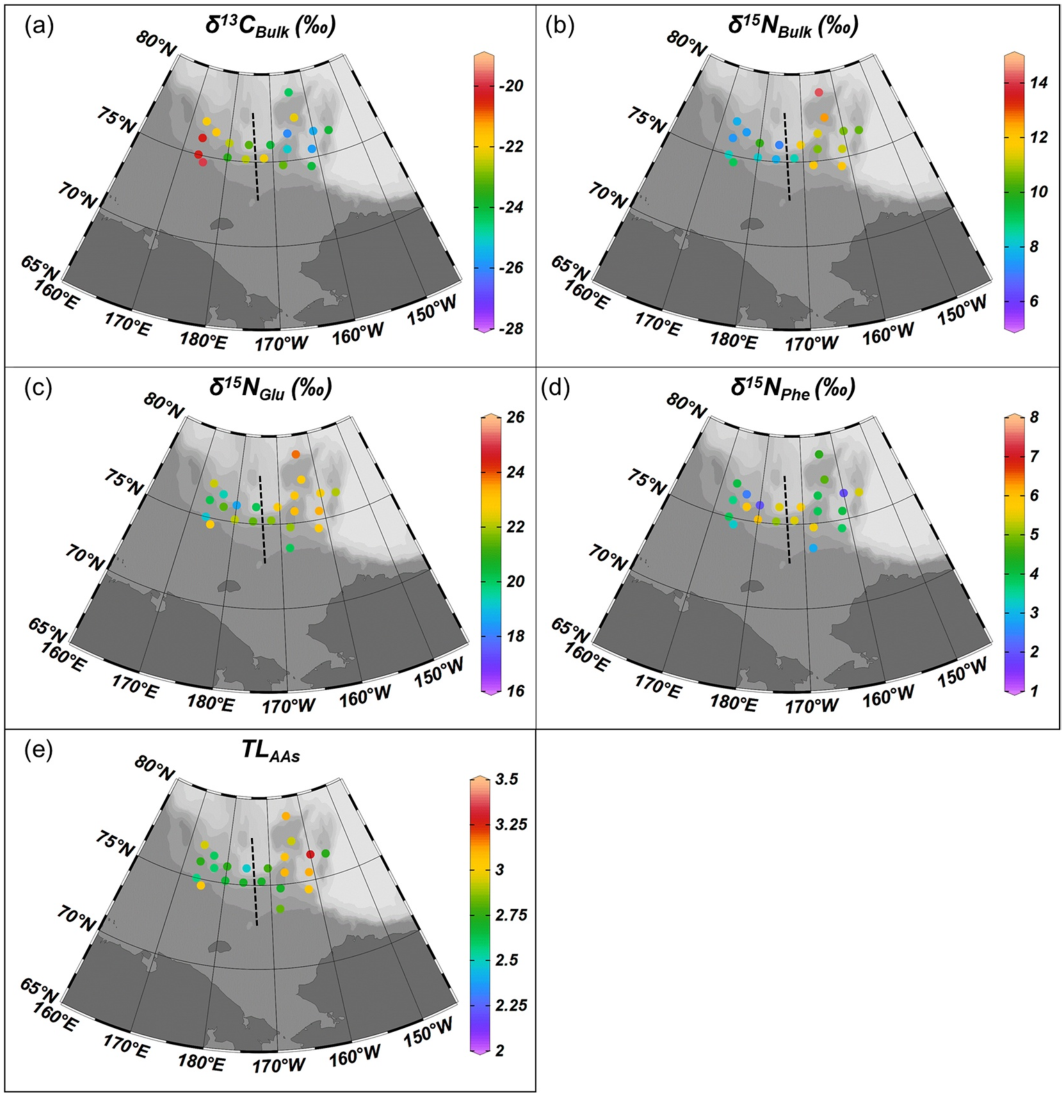

Figure 6. Spatial distribution of $\delta^{13}C_{Bulk}$ (a), $\delta^{15}N_{Bulk}$ (b), $\delta^{15}N_{Glu}$ (c), $\delta^{15}N_{Phe}$ (d), and TL_{AAs} (e) values of *C. hyperboreus*. Black dashed lines in each subfigure are for separating NESS and NCS. NCS, northern Chukchi Sea; NESS, northern-East Siberian Sea.

Copepods generally take advantage of the most common prey (phytoplankton) available to them (Campbell et al., 2016). However, when phytoplankton biomass is low and dominated by small cells, protozooplankton contribute more significantly to copepod diets (Calbet & Saiz, 2005; Dutz & Peters, 2008). *C. hyperboreus* likely ingest protozooplankton or other large organic particles in the NCS, which in our study was dominated by small phytoplankton. Therefore, higher TL_{AA} values for *C. hyperboreus* and low abundance levels of protozooplankton in the NCS can be expected due to the grazing effect. In addition, the TL_{AA} values of *C. hyperboreus* were nearly the same for both melted and frozen stations, indicating few differences in stable isotope signatures, even though *C. hyperboreus* exhibited slightly lower C20:5(n-3) proportions in melted stations compared with frozen stations (Figure 5b).

During our field observations, a high contribution of micro-chl *a* was found, suggesting higher contributions of diatoms for the entire primary production in the NESS stations. *C. hyperboreus* in the NESS can feed more on diatoms, resulting in higher C20:5(n-3) contents compared with the NCS (Figure 8). As a result, the TL_{AA} variation in *C. hyperboreus* can be correlated with C20:5(n-3) proportions, reflecting greater

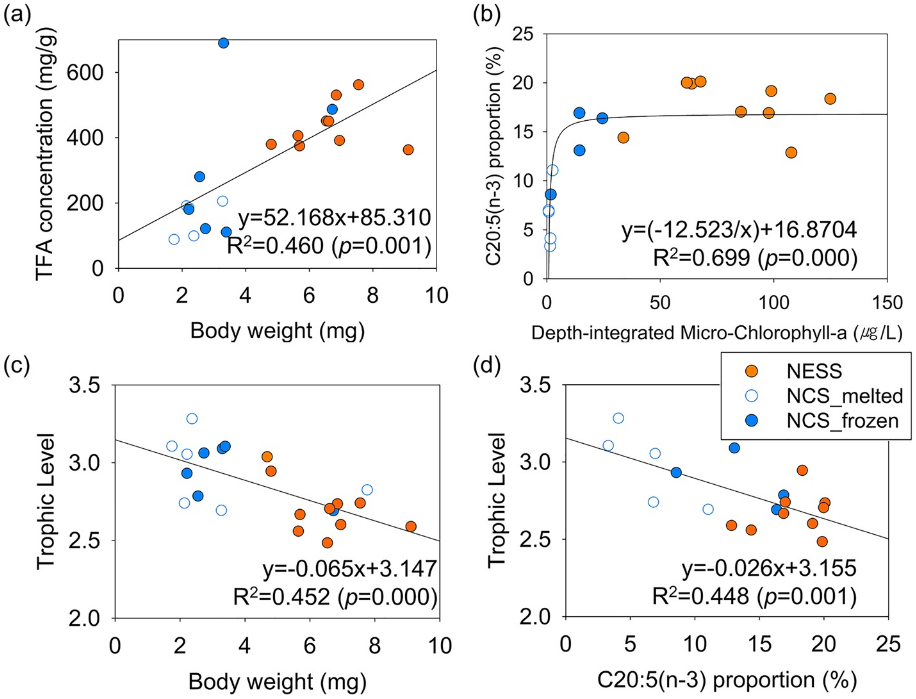

Figure 7. Regressions using body weight versus TFA concentration (a), depth-integrated chl *a* versus C20:5(n-3) contents (b), body weight versus trophic level (c), and C20:5(n-3) contents versus trophic level (d). TFA, total fatty acid.

diatom abundance as an available diet (Figure 7d). These trophic dynamics of *C. hyperboreus* can be caused by the spatial variation of phytoplankton composition, suggesting different planktonic food webs between the NESS and NCS in summer.

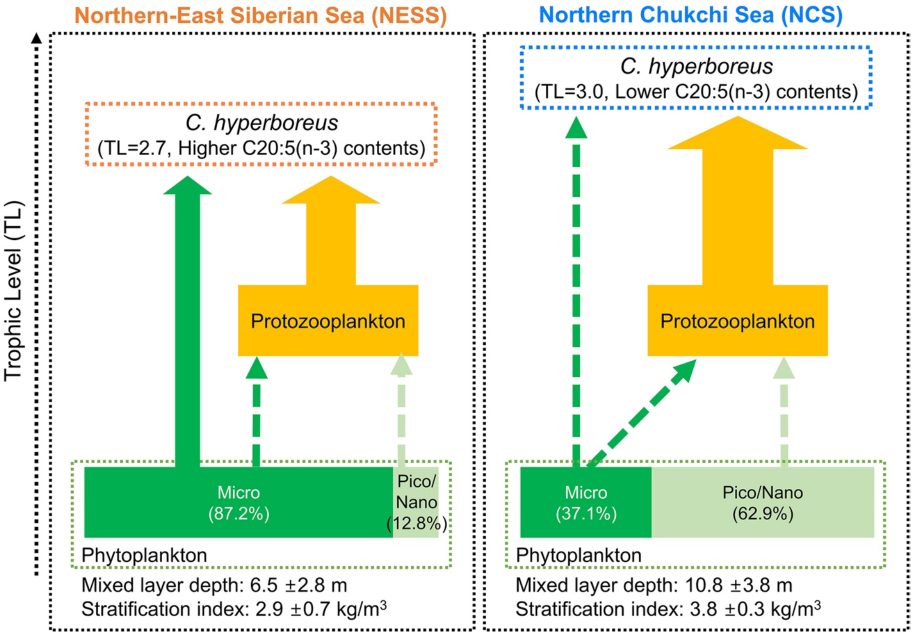

Figure 8. A conceptual illustration of TL distribution between the northeastern Siberian Sea and northern Chukchi Sea. Proportions of micro-chl *a* concentrations (depth-integrated) in the NESS and NCS are shown in the area of each box. The thickness of each arrow is the relative amount of diets consumed by *C. hyperboreus*, leading to spatial variation in their TL values. NCS, northern Chukchi Sea; NESS, northern-East Siberian Sea; TL, trophic level.

The TL_{AA} of *C. hyperboreus* was determined to explore the trophic dynamics and diet composition between the NCS and NESS in the Pacific region of the Arctic Ocean in the summer of 2018. We found that higher TL_{AA} values for *C. hyperboreus* in the NCS resulted from larger diet contribution of protozooplankton, compared to the NESS. The C20:5(n-3) contents of *C. hyperboreus* showed lower abundance in the NCS than in NESS, suggesting different contribution rates of diatoms to phytoplankton communities. Both FA and δ^{15}N-AAs analysis of *C. hyperboreus* provided useful information to understand shifts in trophic levels of *C. hyperboreus* and its diet sources. The feeding difference of *C. hyperboreus* was triggered by differences in surface water stratification between the NESS and NCS. In this study, *C. hyperboreus,* which is a filter-feeding copepod that occurs across the entire Arctic Ocean, may be a useful indicator organism for tracing trophic dynamics in planktonic food webs.

Data Availability Statement

All datasets for this research are available in this paper, supplementary information files, and Korea Arctic Ocean-data System (KAOS, https://kaos.kopri.re.kr).

Acknowledgments
The authors appreciate the contributions of all members of the cruise for sample collection. The authors thank careful assistant of the captain and crew of the research vessel (R/V ARAON) in our field work. This research was a part of a project titled "Korea-Arctic Ocean Observing System (K-AOOS), Korea Polar Research Institute (KOPRI, 20160245)," funded by Ministry of Oceans and Fisheries, Korea.

References

Anderson, L. G., Björk, G., Holby, O., Jutterström, S., Mörth, C. M., O'Regan, M., et al. (2017). Shelf-basin interaction along the east Siberian Sea. *Ocean Science*, *13*(2), 349–363. https://doi.org/10.5194/os-13-349-2017

Arrigo, K. R., & van Dijken, G. L. (2015). Continued increases in Arctic ocean primary production. *Progress in Oceanography*, *136*, 60–70. https://doi.org/10.1016/j.pocean.2015.05.002

Bowes, R. E., & Thorp, J. H. (2015). Consequences of employing amino acid vs. bulk-tissue, stable isotope analysis: A laboratory trophic position experiment. *Ecosphere*, *6*(1), 1–12. https://doi.org/10.1890/es14-00423.1

Boyd, C. M. (1976). Selection of particle sizes by filter-feeding copepods: A plea for reason. *Limnology & Oceanography*, *21*(1), 175–180. https://doi.org/10.4319/lo.1976.21.1.0175

Calbet, A., & Saiz, E. (2005). The ciliate-copepod link in marine ecosystems. *Aquatic Microbial Ecology*, *38*(2), 157–167. https://doi.org/10.3354/ame038157

Campbell, R. G., Ashjian, C. J., Sherr, E. B., Sherr, B. F., Lomas, M. W., Ross, C., et al. (2016). Mesozooplankton grazing during spring sea-ice conditions in the eastern Bering Sea. *Deep Sea Research Part II: Topical Studies in Oceanography*, *134*, 157–172. https://doi.org/10.1016/j.dsr2.2015.11.003

Campbell, R. G., Sherr, E. B., Ashjian, C. J., Plourde, S., Sherr, B. F., Hill, V., & Stockwell, D. A. (2009). Mesozooplankton prey preference and grazing impact in the western Arctic ocean. *Deep Sea Research Part II: Topical Studies in Oceanography*, *56*(17), 1274–1289. https://doi.org/10.1016/j.dsr2.2008.10.027

Chikaraishi, Y., Ogawa, N. O., Kashiyama, Y., Takano, Y., Suga, H., Tomitani, A., et al. (2009). Determination of aquatic food-web structure based on compound-specific nitrogen isotopic composition of amino acids. *Limnology and Oceanography: Methods*, *7*(11), 740–750. https://doi.org/10.4319/lom.2009.7.740

Choi, H., Ha, S.-Y., Lee, S., Kim, J.-H., & Shin, K.-H. (2020). Trophic dynamics of zooplankton before and after polar night in the Kongsfjorden (Svalbard): Evidence of trophic position estimated by δ^{15}N analysis of amino acids. *Frontiers in Marine Science*, *7*. https://doi.org/10.3389/fmars.2020.00489

Cleary, A. C., Søreide, J. E., Freese, D., Niehoff, B., & Gabrielsen, T. M. (2017). Feeding by Calanus glacialis in a high arctic fjord: Potential seasonal importance of alternative prey. *ICES Journal of Marine Science*, *74*(7), 1937–1946. https://doi.org/10.1093/icesjms/fsx106

Conover, R. J. (1988). Comparative life histories in the genera Calanus and Neocalanus in high latitudes of the northern hemisphere. *Hydrobiologia*, *167*(1), 127–142. https://doi.org/10.1007/978-94-009-3103-9_11

Coupel, P., Jin, H. Y., Joo, M., Horner, R., Bouvet, H. A., Sicre, M.-A., et al. (2012). Phytoplankton distribution in unusually low sea ice cover over the Pacific Arctic. *Biogeosciences*, *9*, 4835–4850. https://doi.org/10.5194/bg-9-4835-2012

Coupel, P., Ruiz-Pino, D., Sicre, M. A., Chen, J. F., Lee, S. H., Schiffrine, N., et al. (2015). The impact of freshening on phytoplankton production in the pacific Arctic ocean. *Progress in Oceanography*, *131*, 113–125. https://doi.org/10.1016/j.pocean.2014.12.003

Dahl, T. M., Lydersen, C., Kovacs, K. M., Falk-Petersen, S., Sargent, J., Gjertz, I., & Gulliksen, B. (2000). Fatty acid composition of the blubber in white whales (Delphinapterus leucas). *Polar Biology*, *23*(6), 401–409. https://doi.org/10.1007/s003000050461

Dutz, J., & Peters, J. (2008). Importance and nutritional value of large ciliates for the reproduction of Acartia clausi during the post spring-bloom period in the North Sea. *Aquatic Microbial Ecology*, *50*(3), 261–277. https://doi.org/10.3354/ame01168

Falk-Petersen, S., Mayzaud, P., Kattner, G., & Sargent, J. R. (2009). Lipids and life strategy of Arctic Calanus. *Marine Biology Research*, *5*(1), 18–39. https://doi.org/10.1080/17451000802512267

Folch, J., Lees, M., & Stanley, G. H. S. (1957). A simple method for the isolation and purification of total lipides from animal tissues. *Journal of Biological Chemistry*, *226*(1), 497–509. https://doi.org/10.1016/s0021-9258(18)64849-5

Frost, B. W. (1972). Effects of size and concentration of food particles on the feeding behavior of the marine planktonic Copepod Calanus pacificus 1. *Limnology & Oceanography*, *17*(6), 805–815. https://doi.org/10.4319/lo.1972.17.6.0805

Garrido, J. L., & Medina, I. (1994). One-step conversion of fatty acids into their 2-alkenyl-4,4-dimethyloxazoline derivatives directly from total lipids. *Journal of Chromatography A*, *673*(1), 101–105. https://doi.org/10.1016/0021-9673(94)87062-4

Graeve, M., Albers, C., & Kattner, G. (2005). Assimilation and biosynthesis of lipids in Arctic Calanus species based on feeding experiments with a 13C labelled diatom. *Journal of Experimental Marine Biology and Ecology*, *317*(1), 109–125. https://doi.org/10.1016/j.jembe.2004.11.016

Grigor, J. J., Marais, A. E., Falk-Petersen, S., & Varpe, Ø. (2015). Polar night ecology of a pelagic predator, the chaetognath Parasagitta elegans. *Polar Biology*, *38*(1), 87–98. https://doi.org/10.1007/s00300-014-1577-8

Hannides, C. C. S., Popp, B. N., Landry, M. R., & Graham, B. S. (2009). Quantification of zooplankton trophic position in the north Pacific Subtropical Gyre using stable nitrogen isotopes. *Limnology & Oceanography*, *54*(1), 50–61. https://doi.org/10.4319/lo.2009.54.1.0050

He, J., Zhang, F., Lin, L., Ma, Y., & Chen, J. (2012). Bacterioplankton and picophytoplankton abundance, biomass, and distribution in the western Canada basin during summer 2008. *Deep Sea Research Part II: Topical Studies in Oceanography*, *81–84*, 36–45. https://doi.org/10.1016/j.dsr2.2012.08.018

Huntley, M., & Tande, K. (1987). On the trophic fate of Phaeocystis pouchetii (Hariot). II. Grazing rates of Calanus hyperboreus (Krøyer) on diatoms and different size categories of Phaeocystis pouchetii. *Journal of Experimental Marine Biology and Ecology*, *110*(3), 197–212. https://doi.org/10.1016/0022-0981(87)90001-3

Jiang, Y., Yang, E. J., Min, J.-O., Kang, S.-H., & Lee, S. (2013). Using pelagic ciliated microzooplankton communities as an indicator for monitoring environmental condition under impact of summer sea-ice reduction in western Arctic ocean. *Ecological Indicators*, *34*, 380–390. https://doi.org/10.1016/j.ecolind.2013.05.026

Joo, H. M., Lee, S. H., Jung, S. W., Dahms, H.-U., & Lee, J. H. (2012). Latitudinal variation of phytoplankton communities in the western Arctic ocean. *Deep Sea Research Part II: Topical Studies in Oceanography*, *81*, 3–17. https://doi.org/10.1016/j.dsr2.2011.06.004

Kelly, J., & Scheibling, R. (2012). Fatty acids as dietary tracers in benthic food webs. *Marine Ecology Progress Series*, *446*, 1–22. https://doi.org/10.3354/meps09559

Kim, H.-J., Kim, H. J., Yang, E.-J., Cho, K.-H., Jung, J., Kang, S.-H., et al. (2021). Temporal and spatial variations in particle fluxes on the Chukchi sea and east Siberian sea slopes from 2017 to 2018. *Frontiers in Marine Science*, *7*(1140). https://doi.org/10.3389/fmars.2020.609748

Kruse, S., Hagen, W., & Bathmann, U. (2010). Feeding ecology and energetics of the Antarctic chaetognaths Eukrohnia hamata, E. bathypelagica and E. bathyantarctica. *Marine Biology*, *157*(10), 2289–2302. https://doi.org/10.1007/s00227-010-1496-3

Lalande, C., Nöthig, E. M., & Fortier, L. (2019). Algal export in the Arctic ocean in times of global warming. *Geophysical Research Letters*, *46*(11), 5959–5967. https://doi.org/10.1029/2019gl083167

Lee, M.-C., Choi, H., Park, J. C., Yoon, D.-S., Lee, Y., Hagiwara, A., et al. (2020). A comparative study of food selectivity of the benthic copepod Tigriopus japonicus and the pelagic copepod Paracyclopina nana: A genome-wide identification of fatty acid conversion genes and nitrogen isotope investigation. *Aquaculture*, *521*, 734930. https://doi.org/10.1016/j.aquaculture.2020.734930

Lee, Y., Min, J.-O., Yang, E. J., Cho, K.-H., Jung, J., Park, J., et al. (2019). Influence of sea ice concentration on phytoplankton community structure in the Chukchi and east Siberian Seas, Pacific Arctic ocean. *Deep Sea Research Part I: Oceanographic Research Papers*, *147*, 54–64. https://doi.org/10.1016/j.dsr.2019.04.001

Levinsen, H., Turner, J., Nielsen, T., & Hansen, B. (2000). On the trophic coupling between protists and copepods in arctic marine ecosystems. *Marine Ecology Progress Series*, *204*, 65–77. https://doi.org/10.3354/meps204065

Li, W. K., McLaughlin, F. A., Lovejoy, C., & Carmack, E. C. (2009). Smallest algae thrive as the Arctic ocean freshens. *Science*, *326*(5952). 539. https://doi.org/10.1126/science.1179798

Matsuno, K., Ichinomiya, M., Yamaguchi, A., Imai, I., & Kikuchi, T. (2014). Horizontal distribution of microprotist community structure in the western Arctic ocean during late summer and early fall of 2010. *Polar Biology*, *37*(8), 1185–1195. https://doi.org/10.1007/s00300-014-1512-z

McLaughlin, F., Carmack, E., Proshutinsky, A., Krishfield, R., Guay, C., Yamamoto-Kawai, M., et al. (2011). The rapid response of the Canada Basin to climate forcing: From bellwether to alarm bells. *Oceanography*, *24*(3), 146–159. https://doi.org/10.5670/oceanog.2011.66

McLaughlin, F. A., & Carmack, E. C. (2010). Deepening of the nutricline and chlorophyll maximum in the Canada basin interior, 2003–2009. *Geophysical Research Letters*, *37*(24). https://doi.org/10.1029/2010gl045459

McMahon, K. W., & McCarthy, M. D. (2016). Embracing variability in amino acid δ^{15}N fractionation: Mechanisms, implications, and applications for trophic ecology. *Ecosphere*, *7*(12), e01511. https://doi.org/10.1002/ecs2.1511

McMeans, B. C., Arts, M. T., Rush, S. A., & Fisk, A. T. (2012). Seasonal patterns in fatty acids of Calanus hyperboreus (Copepoda, Calanoida) from Cumberland Sound, Baffin Island, Nunavut. *Marine Biology*, *159*(5), 1095–1105. https://doi.org/10.1007/s00227-012-1889-6

Minagawa, M., & Wada, E. (1984). Stepwise enrichment of 15N along food chains: Further evidence and the relation between δ^{15}N and animal age. *Geochimica et Cosmochimica Acta*, *48*(5), 1135–1140. https://doi.org/10.1016/0016-7037(84)90204-7

Nishino, S., Itoh, M., Williams, W. J., & Semiletov, I. (2013). Shoaling of the nutricline with an increase in near-freezing temperature water in the Makarov Basin. *Journal of Geophysics Research: Oceans*, *118*(2), 635–649. https://doi.org/10.1029/2012jc008234

Ohkouchi, N., Chikaraishi, Y., Close, H. G., Fry, B., Larsen, T., Madigan, D. J., et al. (2017). Advances in the application of amino acid nitrogen isotopic analysis in ecological and biogeochemical studies. *Organic Geochemistry*, *113*, 150–174. https://doi.org/10.1016/j.orggeochem.2017.07.009

Sargent, J. R., Bell, J. G., Bell, M. V., Henderson, R. J., & Tocher, D. R. (1995). Requirement criteria for essential fatty acids. *Journal of Applied Ichthyology*, *11*(3-4), 183–198. https://doi.org/10.1111/j.1439-0426.1995.tb00018.x

Scott, C., Kwasniewski, S., Falk-Petersen, S., & Sargent, J. (2002). Species differences, origins and functions of fatty alcohols and fatty acids in the wax esters and phospholipids of Calanus hyperboreus, C. glacialis and C. finmarchicus from Arctic waters. *Marine Ecology Progress Series*, *235*, 127–134. https://doi.org/10.3354/meps235127

Semiletov, I., Dudarev, O., Luchin, V., Charkin, A., Shin, K. H., & Tanaka, N. (2005). The east Siberian sea as a transition zone between Pacific-derived waters and Arctic shelf waters. *Geophysical Research Letters*, *32*(10). https://doi.org/10.1029/2005gl022490

Spitzer, V. (1996). Structure analysis of fatty acids by gas chromatography—low resolution electron impact mass spectrometry of their 4,4-dimethyloxazoline derivatives—A review. *Progress in Lipid Research*, *35*(4), 387–408. https://doi.org/10.1016/s0163-7827(96)00011-2

Spreen, G., Kaleschke, L., & Heygster, G. (2008). Sea ice remote sensing using AMSR-E 89-GHz channels. *Journal of Geophysical Research*, *113*(C2). https://doi.org/10.1029/2005jc003384

Søreide, J. E., Falk-Petersen, S., Hegseth, E. N., Hop, H., Carroll, M. L., Hobson, K. A., & Blachowiak-Samolyk, K. (2008). Seasonal feeding strategies of Calanus in the high-Arctic Svalbard region. *Deep Sea Research Part II: Topical Studies in Oceanography*, *55*(20), 2225–2244. https://doi.org/10.1016/j.dsr2.2008.05.024

Søreide, J. E., Hop, H., Carroll, M. L., Falk-Petersen, S., & Hegseth, E. N. (2006). Seasonal food web structures and sympagic-pelagic coupling in the European Arctic revealed by stable isotopes and a two-source food web model. *Progress in Oceanography*, *71*(1), 59–87.

Søreide, J. E., Leu, E., Berge, J., Graeve, M., & Falk-Petersen, S. (2010). Timing of blooms, algal food quality and Calanus glacialis reproduction and growth in a changing Arctic. *Global Change Biology*, *16*(11), 3154–3163. https://doi.org/10.1111/j.1365-2486.2010.02175.x

Tremblay, G., Belzile, C., Gosselin, M., Poulin, M., Roy, S., & Tremblay, J. (2009). Late summer phytoplankton distribution along a 3,500 km transect in Canadian Arctic waters: Strong numerical dominance by picoeukaryotes. *Aquatic Microbial Ecology*, *54*(1), 55–70. https://doi.org/10.3354/ame01257

Yang, E. J., Ha, H. K., & Kang, S.-H. (2015). Microzooplankton community structure and grazing impact on major phytoplankton in the Chukchi sea and the western Canada basin, Arctic ocean. *Deep Sea Research Part II: Topical Studies in Oceanography*, *120*, 91–102. https://doi.org/10.1016/j.dsr2.2014.05.020

Zhuang, Y., Jin, H., Chen, J., Li, H., Ji, Z., Bai, Y., & Zhang, T. (2018). Nutrient and phytoplankton dynamics driven by the Beaufort Gyre in the western Arctic Ocean during the period 2008-2014. *Deep Sea Research Part I: Oceanographic Research Papers*, *137*, 30–37. https://doi.org/10.1016/j.dsr.2018.05.002